



HAL
open science

Optimized integration of a modular motor driver in a low voltage high power, open winding synchronous machine

Alexandre Siccardi, Charles Joubert, Christian Martin, Ali Makki, Louis Dassonville, Benjamin Coelho Gaspar

► To cite this version:

Alexandre Siccardi, Charles Joubert, Christian Martin, Ali Makki, Louis Dassonville, et al.. Optimized integration of a modular motor driver in a low voltage high power, open winding synchronous machine. PCIM; Conference for Power Electronics, Intelligent Motion, Renewable Energy and Energy Management, May 2023, Nuremberg, Germany. 10.30420/566091297 . hal-04289958

HAL Id: hal-04289958

<https://hal.science/hal-04289958v1>

Submitted on 16 Nov 2023

HAL is a multi-disciplinary open access archive for the deposit and dissemination of scientific research documents, whether they are published or not. The documents may come from teaching and research institutions in France or abroad, or from public or private research centers.

L'archive ouverte pluridisciplinaire **HAL**, est destinée au dépôt et à la diffusion de documents scientifiques de niveau recherche, publiés ou non, émanant des établissements d'enseignement et de recherche français ou étrangers, des laboratoires publics ou privés.

Optimized integration of a modular motor driver in a low voltage high power, open winding synchronous machine

SICCARDI Alexandre^{1,2}, JOUBERT Charles¹, MARTIN Christian¹, MAKKI Ali², DASSONVILLE Louis^{1,2}, COELHO GASPAR Benjamin^{1,2}

¹ Univ Lyon, Université Claude Bernard Lyon 1, INSA Lyon, Ecole Centrale de Lyon, CNRS, Ampère, UMR5005, 69622 Villeurbanne, France

² KEEP MOTION, 3 Z.A de la Noyeree, 38200 LUZINAY, France

Corresponding author: SICCARDI Alexandre, Alexandre.siccardi@keep-motion.com

Speaker: SICCARDI Alexandre, Alexandre.siccardi@keep-motion.com

Abstract

This paper provides an optimization method for integrated modular motor driver (IMMD) with open-winding synchronous motors. This method can be used on different topologies of open winding machines and can be applied to others stator configurations. The concept of IMMD as well as different integration works are presented. All possible inverter integration methods are described with three of them experimented in the literature. Finally, an application of the optimization process is detailed. It allows to optimize the use of the integrated modular inverter volume, while respecting the physical, thermal, and mechanical constraints of the motor and the components.

1 Introduction

For several years, sales of electric vehicles have been growing rapidly over the world. The higher power density requirements have challenged the manufacturing methods of permanent magnet synchronous motors (PMSM). In these applications, the supply voltage is limited by the battery and the speed can exceed 6,000 rpm for an ever-increasing torque demand. The resulting high phase currents force manufacturers to increase the conductor cross-section. This implies a reduction in the winding turn number and a lower fill factor [1], which leads to higher losses. In addition, the increased wire diameter is responsible for additional Joule losses due to the skin effect. Existing solutions consisting of dividing the windings into several parallel wires imply technological difficulties for large-scale industrialization (burying in the slots and soldering the connections).

Several solutions are possible to overcome the winding challenges and gain power density. The most common method, doubling the battery voltage, reduces the current in the motor windings and increases the motor power in the flux-weakening region. However, the motor design becomes more complicated because of the additional insulation required to limit partial discharges. Another method found in mid high-end cars is to use multiple motors to power the vehicle such as the Tesla Model S dual motor or the Koenigsegg Gemera.

However, another method is to increase the number of phases in the motor. In applications where the supply voltage is limited, polyphase motors are a solution to reduce the phase current. In this case the diameter of each conductor is reduced, which increases the copper fill factor of the stator and thus the efficiency of the motor. In addition, the increase in the number of phases in PMSMs leads to better reliability [2].

To further improve the reliability of multiphase motors, the windings of each phase are divided into subgroups and driven by different converters. The most reliable system is achieved when each winding is supplied independently by an inverter. However, such electric motors must be powered by specific converters. These converters can be integrated into the motor to improve the power density of the drive system and are called Integrated Modular Motor Drives (IMMD).

In the literature, many works present prototypes of multiphase motors powered by IMMD [3-8]. However, none of them were designed to independently drive the coils of an open wound permanent magnet synchronous motor (OW-PMSM), with a full bridge inverter. Using a single-phase inverter per winding with a distributed control law in an OW-PMSM achieves the highest level of reliability for the drive train [9].

2 Benefits and challenges of IMMD

Introduced in [10], the integrated motor driver (IMD) concept emerged in the late 20th century. Today, this technology is widely used in low- to medium-power fan applications, but it faces difficulties in being implemented in other variable speed applications. Compared to a conventional variable speed drive, the integration of electronics into the motor offers many advantages, such as higher power density. Nevertheless, IMD faces two main challenges, which are thermal management and component miniaturization. The optimization of thermal management can be done in 3 aspects:

- Utilization of electronic components that can operate at high temperatures.
- Reduction of Joule losses in the power electronics of the inverter.
- Improvement of the heat transfer between the components and the heatsink to evacuate the losses.

The other factor limiting integration is the size of the power components. In voltage source inverters, DC bus decoupling capacitors ensure a stable DC bus voltage, especially during transistors switching. These capacitors can represent up to 30% of the total volume of the inverter [11]. The reduction of the required capacitance is therefore of great interest for the integration of the inverter into the motor. This can be done by using an interleaving method or by increasing the number of phases in the case of a multiphase motor. Another possibility is to increase the switching

frequency to reduce the required capacity. However, this method, in addition to increasing the switching frequency, is limited by the capacitor technology. When the switching frequency is increased beyond a frequency threshold, the required operating current overcomes the capacitance, and the capacitor volume no longer decreases. By working on these key points, the size of the power circuit can be minimized, and the power density of the electronics increased.

3 Electronic integration in the motor

Mechanical parts that constitute an electric motor are the rotor, stator, shaft, bearings, stator sleeve, and front and rear end caps. All these parts are essential to the proper operation of an electric motor. To integrate the inverter electronics into the motor and keep the length of the coil head leads as short as possible, electronics can be integrated in the area represented by the green cylinder in figure 1. The modular inverter to be integrated consists of several identical modules. Integration volume can therefore be divided into equal parts, shown in blue in figure 1, each part being a slice of the cylinder defined by the polar pitch of the stator windings.

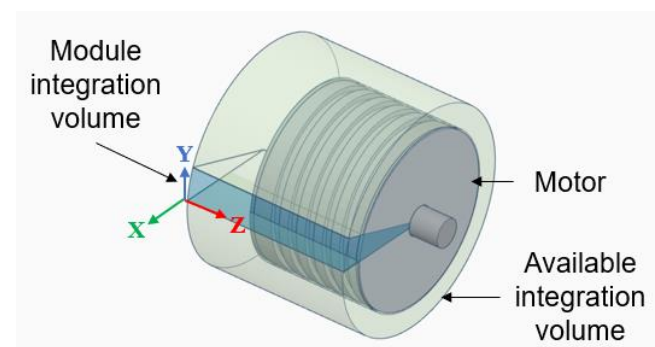


Fig. 1 Volume available for IMMD integration in green and volume for integration of an IMMD module in the case of an open winding motor in blue.

The orthonormal reference $(\vec{x}, \vec{y}, \vec{z})$ of an inverter module is defined with \vec{x} collinear to \vec{r} the radius of the cylindrical reference $(\vec{r}, \vec{\theta}, \vec{z})$ of the integration volume. The PCBs can be mounted in all three planes of the reference frame $(\vec{x}, \vec{y}, \vec{z})$ either inside the stator diameter or outside (over the sleeve). In the first case, the motor diameter is a constraint, and the integration of the electronics will impact the overall length of the machine, in the second case it is the opposite. There are therefore six different ways of integrating the electronics into the motor, as represented in figure 2. Methods A,

B and C in the first row are the methods of integration inside the stator diameter that increase the length of the machine, while methods D, E and F in the second row are those outside the stator that increase the diameter. The three columns represent, in order, the orientation of the boards in the (\vec{x}, \vec{y}) , (\vec{y}, \vec{z}) and (\vec{x}, \vec{z}) planes.

Method A was introduced in [3] and used in [4] and [5]. The PCBs of the inverter modules are mounted in a circle above the backplane in the (\vec{x}, \vec{y}) plane. In this work, the stator is connected in a star configuration, so each winding is fed from a half-bridge. With this method, the cooling of the power components can be done through the rear end cap, or through an additional end cap above the IMMD. Multiple PCBs can be stacked along the \vec{z} -axis to increase the area of a module. However, the A method is limited by the area of a module, which depends on the pole pitch and the stator diameter. The use of this method is only effective if the area of the power board and the heat sink fit on the area of a module. This method is therefore suitable for motors with few poles in the stator and low powers.

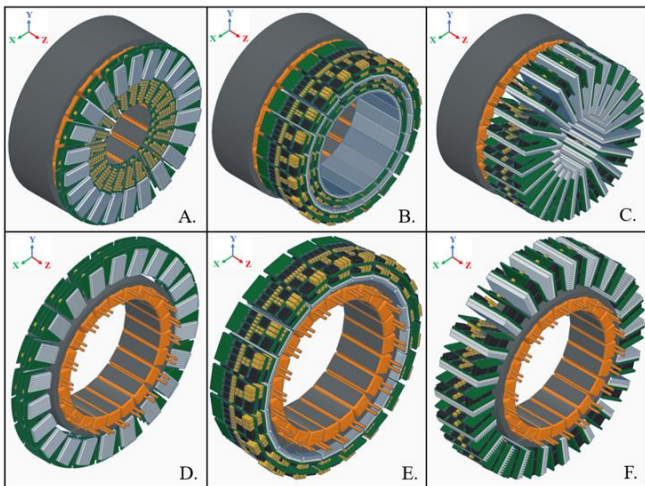


Fig. 2 The six approaches of integrating an IMMD into an electric motor.

In method B, the boards are mounted on the (\vec{y}, \vec{z}) plane in the stator diameter. The first board is fixed on the stator sleeve, being able to benefit from efficient heat dissipation. The area of the PCBs can be increased by extending them in the \vec{z} direction, but the width is limited by the pole pitch and the stator diameter. It is possible to stack the boards in the \vec{x} direction, the stacking causes a reduction in the width of the PCBs since the radius of the circle on which these boards are placed decreases. Beyond a certain number, stacking is no longer

possible since the width of a board no longer allows for the placement of components. Due to the strong constraints on the width of the PCBs, the B method does not achieve a high-power density by volume for IMMD.

Method C has been used in [1], [8] and [12]. The PCBs are mounted internally on stator on the (\vec{x}, \vec{z}) plane. Unlike methods A and B, this method cannot use mechanical parts to dissipate heat from the power components. Therefore, the heatsink must be integrated into the module, which makes thermal management more complex. The length of the PCBs can be increased in the \vec{z} -axis, while the width is determined by the pole pitch and diameter of the stator, the height of the heatsink, and the spacing between the boards. It is possible to stack several cards, however the width of the pole pitch is a constraint on the number of cards that can be stacked. This method is therefore more complex to implement than the previous methods, but it provides a large routing and dissipation area for the module.

Method D is like the method A, the boards are mounted in the same plane (\vec{x}, \vec{y}) outside the stator. Unlike method A, the area of the boards can be adapted by increasing the overall diameter of the machine. In this configuration, the cooling can be done on the front and rear end plate. This method is most effective on motors with short lengths and large diameters such as discoid motors. Indeed, even though the PCBs can be stacked in the \vec{z} direction, the IMMD design is more complex when the number of stacked boards is large. In the case of a short discoid machine where the overall diameter is not a constraint, it is possible to realize large area PCBs where the stacking allows the entire length of the stator to be used. This allows a high-power density to be achieved.

In method E presented in [6], the PCBs are mounted on the outside of the stator, in the (\vec{y}, \vec{z}) plane. The boards can be the same length as the stator, providing a large area. It is possible to stack the boards to increase the total area of a module, and unlike method B, the stacked PCBs will have a greater width. The cooling can be done by the stator sleeve or by an external one.

Finally in method F, the PCBs are mounted outside on stator on the (\vec{x}, \vec{z}) plane. As with method C, each module must embed its own heat sink to evacuate heat from the power board. For methods E and F, the length of the stator limits the length of the boards, which is not the case for method D. A machine with a very short length such as a discoid motor may be penalizing for integrating an IMMD according to methods E and F. These methods will

be more suitable for machines with longer lengths, where the overall diameter is not a constraint. However, in an electric motor, the power is proportional to the length of the stator and the square of its diameter. In the case where the design of the motor and the IMMD go together, it will be more interesting to increase the stator diameter and reduce its length. Therefore, the F method is at a disadvantage compared to the C method.

4 Optimizing integration

IMMD integration optimization consists in identifying the best integration method, i.e., the one that maximizes the power density of the motor + inverter assembly. First, the electrical and mechanical characteristics of the electric motor must be identified. This information can be obtained from an existing machine or determined during the design of the motor. Optimizing IMMD integration in parallel with the design of the motor optimizes the whole system power density of the IMMD.

In general, an IMMD combines various electrical functions such as: switching power devices (bridge legs), monitoring and control functions, filtering, instrumentation An example of an inverter block diagram is shown in figure 3. All these functions are interconnected, determining the necessary routing area for an IMMD module. These functions can be distributed over several PCBs interconnected by connectors. The more boards and interconnections there are, the more connectors there will be between the PCBs, which increases the required routing area and electronic volume. For the C and F methods, the height of these connectors influences the width of the PCBs. Some functions have placement constraints. For example, the switching cells must be placed on the power board, which is itself on the heatsink. Also, the DC bus capacitors and drivers should be as close as possible to the transistors to reduce the effects of parasitic inductance.

The optimization process, shown in Figure 4, is an iterative method where the IMMD integration can be tested for each method to determine which method is feasible and achieves the best power density. The preliminary steps are the IMMD electrical design based on the motor requirements and the calculation of the available integration volume. From the electrical design, electronic components are selected, and the required PCB placement area is determined. For each method, the PCB dimensions that can be integrated are

calculated. PCB dimensions can be written as a function whose variables are motor parameters such as stator diameter, number of poles and connector height between the PCBs. If the area required for electronics routing is not achievable, then the IMMD cannot be integrated using this method.

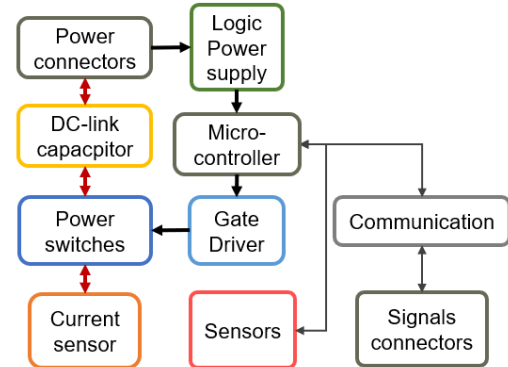


Fig. 3 Block diagram of an IMMD converter module.

The next step is the power board routing of the IMMD module. This board should ideally contain power MOSFETs (or other switching cells), DC-link capacitors, power connectors for DC and AC side, current sensor and eventually MOSFET drivers. If the area is insufficient, components can be moved to a mezzanine board.

Next step is the design of the heat sink that will dissipate the inverter losses. The power to be dissipated includes the losses of the power components and the losses in the power PCB traces. For methods where mechanical parts of the motor are used for heat dissipation, it should be verified that they can transfer the additional heat generated by the inverter and modified if necessary. For methods C and F, the heat sink must be specifically designed. Heatsink dimensions can have an impact on the power board size. The process is iterative, as the length and width of the power board can be modified to achieve optimal space utilization for the power board and heat sink. If the heatsink cannot be integrated into the defined volume, there are several ways to improve it:

- Reduce the Joule losses of the inverter.
- Increase the operating temperature of the transistors.
- Increase the integration volume of the IMMD.
- Change the integration method.

Once the heatsink integration and power dissipation has been verified, the last step is to

complete the inverter routing by integrating the remaining components to the mezzanine boards.

If the surface area of the PCBs is not sufficient for routing, it is possible to increase one of the IMMD integration volume dimensions if it is not constrained. This increased surface area benefits both the heat sink and the power board. The heat dissipation is therefore potentially more efficient since the exchange surface is increased. Depending on the additional surface obtained, it is possible to rearrange the functions between the boards to minimize the electronics volume expansion. Similarly, if dimensions have been changed in the last step, it is possible to repeat the previous steps to attempt to reduce the IMMD's volume.

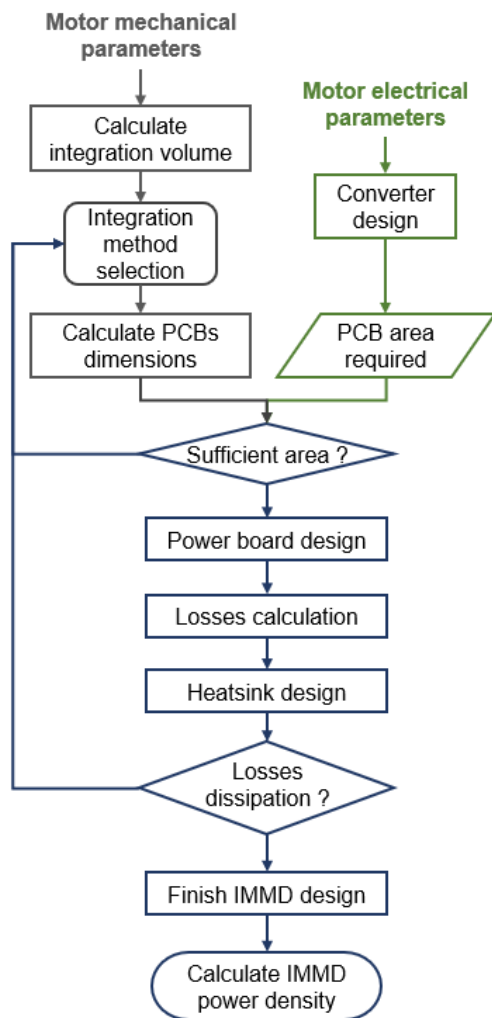


Fig. 4 Proposed IMMD design optimization method.

When the optimization process is complete, the power density volume results of the different IMMD integration methods can be compared to select the

method that achieves the best power density. The optimization process allows (regardless of the integration method, electric motor, and inverter characteristics) to minimize the volume occupied by the IMMD while respecting the physical and thermal limits of the components. A combination of methods can be used, for example, using both the D and F methods. The steps of the optimization process will remain the same, it will only be necessary, for each board and for the heatsink, to define the chosen integration method and to calculate their respective dimensions.

5 Application

The integration method presented in this document has been applied to the IMMD design for an OW-PMSM of 85 kW at peak power supplied by a 48 V battery. The IMMD is composed of 22 modules. To control the OW-PMSM, each module will integrate a microcontroller with a control algorithm and a heatsink. To minimize the IMMD volume, the converter will be divided into 2 boards: One for the control circuit and one for power components (as close as possible from the heatsink). The proposed IMMD is therefore built from perfectly identical modules. The mechanical power and torque curves obtained from the finite element simulation of the polyphase OW-PMSM are presented in Figure 5. According to the results, each converter will have to provide a nominal electrical power of 2.2 kW and a maximum power of 4.1 kW for 30 seconds which represent a maximal current of 150 A_{RMS}. From a mechanical point of view, the entire IMMD must fit in the motor diameter which is equal to 190 mm. Therefore, the selected integration methods are A, B and C from the figure 1.

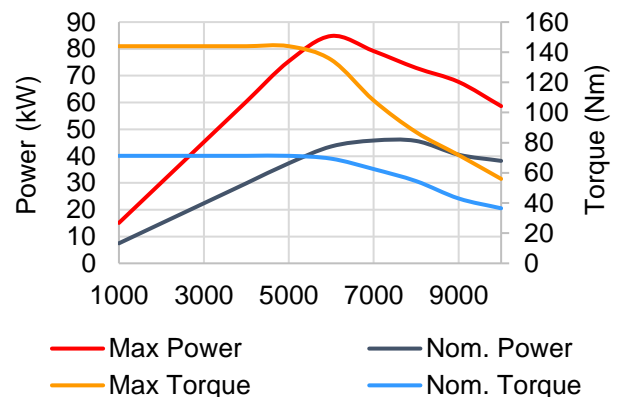


Fig. 5 Mechanical output power and Torque for nominal (65 A_{RMS}) and maximal (150 A_{RMS}) phase current versus rotor speed.

5.1 Converter electrical design

The DC-AC converter has been designed to minimize losses, i.e., maximize efficiency, while ensuring module integration and motor control. The converter circuit diagram is presented in figure 6. The battery voltage V_0 is fixed at 48V while the output current I_{OUT} and output voltage V_{OUT} are fixed by the motor operating point. The converter control, is realized using unipolar modulation (UPWM), detailed in figure 7. This type of modulation allows to double the switching frequency seen by the load, by shifting the switching time by 180 degrees between the two bridge legs. As a result, the output current harmonics are at higher frequencies and therefore better filtered by the motor. The ripple torque of the motor will be consequently reduced.

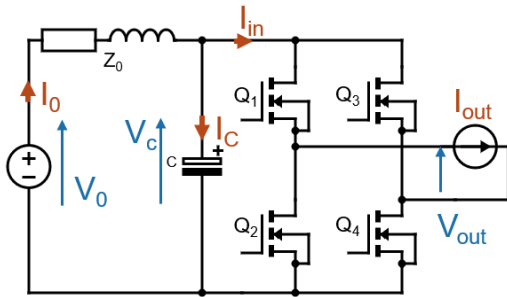


Fig. 6 Circuit diagram of one IMMD converter.

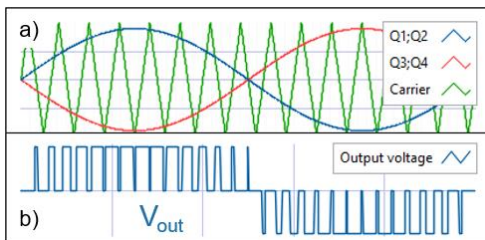


Fig. 7 a) Modulation and carrier waveforms for UPWM and b) Output voltage V_{OUT} waveform.

Power losses in the converter has been calculated using the method detailed in [13]. This method provides a mathematical tool to calculate the power losses in MOSFET-based power converter. The transistor chosen for this converter are the BSC019N08NS5 (Si technology) because they have the lowest $R_{DS(on)}$ MOSFET in TDSO-8 package and a low Q_G which reduce switching losses. To optimize the losses, the converter uses two MOSFET in parallel for each commutation cells. As the conduction losses are proportional to the square of the drain current I_{DS} , the conduction losses are reduced. However, the space for placing the power component is increased. The

use of two transistors in parallel reduces the total losses by 35% compared to a single MOSFET.

The power losses of the converter have been calculated different operating points. The results, shown in figure 8, are plotted as a function of the output current. The conduction losses represent 1.5 W per MOSFET at the nominal point and 7.6 W at maximal power. As the switching losses depending on both the MOSFET drain current and the switching frequency, they are calculated for different frequency. Using a low switching frequency will increase the efficiency of the inverter but may degrade the efficiency, control, and performance of the motor due to the strong current ripples. Furthermore, a lower switching frequency results in a higher capacitance for the DC-link capacitor for a given bus voltage ripple. The total power losses in the inverter are 22 W for the nominal operating point and 85 W for the maximal operating point for a switching frequency of 10 kHz.

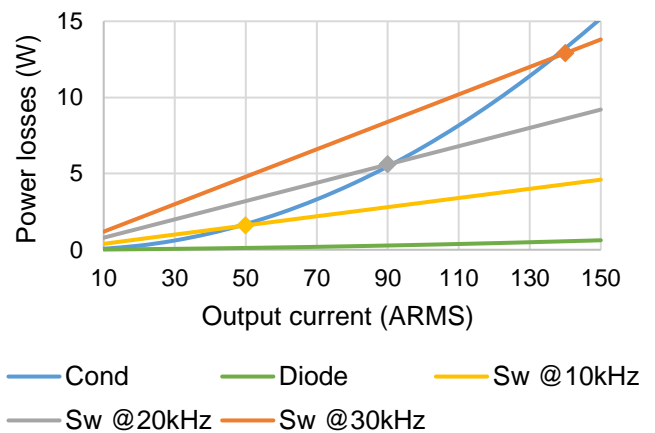


Fig. 8 Detailed losses in a switching cell as a function of current and for different switching frequencies.

To ensure a stable supply voltage, the DC-link capacitor is sized to ensure a maximum ripple bus voltage of 1% in the worst case. The sizing of the DC-link capacitors can be done analytically based on the modulation index and load phase angle [14]. In a single-phase inverter, the input current I_{IN} has three relevant components: a DC component, a low frequency AC current at twice the fundamental frequency and a high frequency component at the switching frequency. To filter the low frequency component, the required capacitance, and consequently the size, is usually high because of the low modulation frequency. However, the large number of phase-shifted converters, operating simultaneously, reduces the required capacitance to filter the input current [15].

A Fourier analysis has been done on the total current in the IMMD DC bus. This current is equal to the sum of all the converter input currents I_{IN} . The waveforms for the input current obtained in the circuit detailed earlier are shown in Figure 9a and the IMMD DC bus current is shown in Figure 9b. The low frequency current at twice the modulation frequency has disappeared by connecting all the converters to the same voltage supply. The resulting current has a DC component and even harmonics, whose first harmonic is equal to twice the switching frequency. Consequently, the capacitance value to filter these harmonics will be greatly reduced. For a switching frequency of 20 kHz, the first current harmonic on the bus will be 40 kHz due to the UPWM modulation.

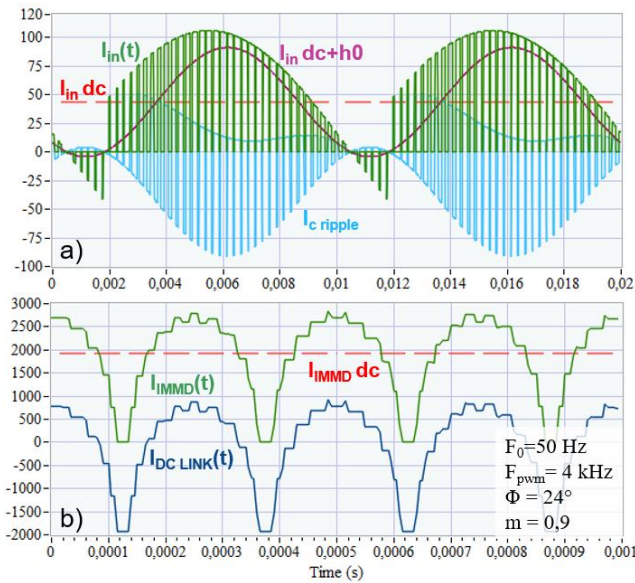


Fig. 9 a) Waveforms of the input current and its three components: the DC current $I_{IN DC}$, the double fundamental frequency harmonic $I_{IN H0}$ and the high frequency ripple current I_C . b) Waveforms of the total current I_{IMMD} in the IMMD with its average value and the current ripple $I_{DC LINK}$.

The DC bus ripple voltage is highest for a load phase angle $\varphi=0^\circ$ and a modulation index $m=0.5$. In this case, the RMS value of the ripple current in one converter at maximum power is 57.5 A_{RMS}, for a current $I_{DC}=53$ A. The required voltage ripple is achieved for a converter DC-link capacitance of 730 μ F. As each board embed a part of the total DC-link capacitor, the total capacitance of the IMMD DC-link is equal to the sum of each converter DC-link capacitance. Similarly, capacitors must be sized to provide a current equal to the $I_{DC LINK}$ current divided by the number of converters.

5.2 Integration method selection

The dimensions of the components obtained during the electrical design are used to select the integration method. The choice of the method meets the following requirements:

- Place all the components of the different electronic circuits.
- Integrate a heatsink capable of dissipating all losses.
- Maximise the power density.

The integration capabilities of electronic boards for methods A, B and C have been studied. The mechanical integration constraints are those of the OW-PMSM studied, i.e., 22 identical modules in a diameter of 190 mm. The constraints used for the electronics are the following: The module will consist of a control board, a 5 mm thick heatsink and a power board, mounted on the heatsink. The estimated placing area is respectively 3500 mm² and 5000 mm² for the control and the power board. The results of the 3 integration methods are detailed in figure 10.

Method	A	B	C
Card length	95 mm	227 mm	77 mm
Power board surface	1288 mm ²	5000 mm ²	5000 mm ²
Control board surface	1288 mm ²	4700 mm ²	3500 mm ²
IMMD total volume	-	6.4 dm ³	2.18 dm ³
Electronic volume	-	2.3 dm ³	1.16 dm ³

Fig. 10 Comparison of PCB sizes and IMMD volume depending on the integration method. The volume of method A was not calculated because it does not allow to integrate the converter.

Method A was not selected because the PCB areas are too small to integrate the power converter. Method B allow a sufficient surface area for the power board but there is a lot of space wasted for the control board. Method C reaches the surface objectives for the control and power board and has the lowest volume. Method C is therefore the most suitable method for the IMMD integration in the motor. This method will be used to realize the converter realization.

5.3 IMMD design integration

Based on the number of stator poles and stator radius, the integration volume of an IMMD module

can be defined. The integration plan of the boards is detailed in figure 11. The heatsink and PCBs are parallel to the z-axis and the dimensions are bounded by the maximum distance between the opposite side of the triangle and the hypotenuse. The position of the module elements on the \vec{y} -axis impacts their maximum length. The further the elements are far from the base of the triangle, the more the length decreases. The board length L in \vec{z} -axis can be calculated from the integration radius R , the PCB height h in \vec{y} -axis and the converter number n using the formula (1). The calculated dimensions are 65x100 mm for the power board and 51x70 mm for the control board.

$$L = R - \frac{h}{\tan\left(\frac{2\pi}{n}\right)} - h \tan\left(\frac{\pi}{2n}\right) \quad (1)$$

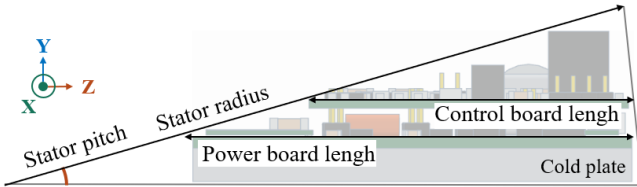


Fig. 11 Integration layout of an IMMD module with the method C.

5.4 PCB traces losses calculation

The power board, designed to integrate the MOSFETs, a current sensor, power connectors and DC-link capacitors, is shown in Figure 12. The power board is an IMS PCB to benefit from a low thermal resistance between the transistors and the cold plate. To obtain sufficient layers on the power board, the capacitors are assembled on a double layer board, soldered directly to the power board.

To evaluate the losses in the traces, the impedance of the traces of the power PCB is characterized and a frequency analysis of the currents in each mesh of the circuit is performed. The method used to calculate the losses in the tracks is described in Figure 13. The impedance calculation is performed by FEM on the 3D CAD model of the power board. Each trace impedance is calculated as a function of frequency, to consider the skin effect and the proximity of the traces. For each traces m , the harmonics h of the currents flowing in it were extracted and the impedance of the trace was interpolated for these frequencies f . The total losses in the power PCB are the sum of the losses

of each track m for each current harmonic h (2). The losses in an m trace for a frequency f corresponding to the harmonic h of current I are the product of the resistance and the square of the current.

$$P_{traces} = \sum_m \sum_h R_{m,h}(f) \cdot I_{m,h}(f)^2 \quad (2)$$

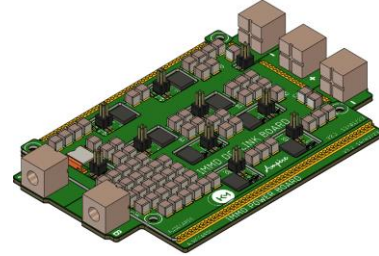


Fig. 12 3D CAD of the IMMD power boards.

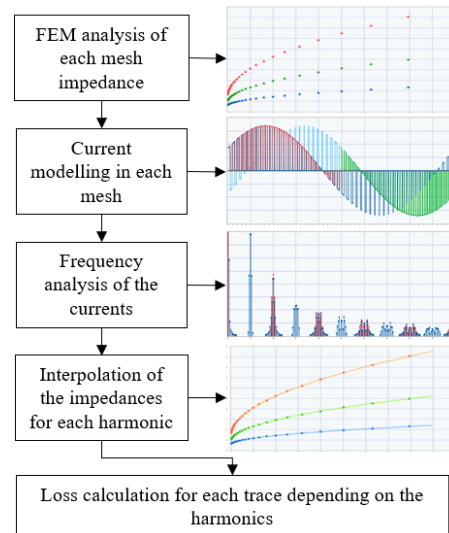


Fig. 13 Method used to evaluate the losses in the power PCB traces.

The trace losses have been added to the convert losses. The total amount of losses to be dissipated by the converter is 103 W at maximum power and 26 W at rated power, for a switching frequency of 10 kHz.

5.5 Thermal design

Power losses dissipation was evaluated by constructing the equivalent thermal circuit of the IMMD module, shown in Figure 14. Each thermal resistance of the different material layers in the system is modelled by a resistance. To simplify the model, it is assumed that heat is transferred vertically to the fluid and that there is no horizontal heat transfer in the layers except in the Al layer corresponding to the PCB substrate which is made of

Aluminium. The copper thermal resistance of the PCB traces was separated into two resistances $R_{TH\ CU1}$ and $R_{TH\ CU2}$. $R_{TH\ CU1}$ is the thermal resistance associated with the copper surface under the MOSFETs to add the contribution of the trace losses P_{TRACES} , to the MOSFET losses P_{INV} . The layers corresponding to resistors $R_{TH\ JC}$, $R_{TH\ SN}$ and $R_{TH\ CU1}$ have the same area S_1 corresponding to the contact area of the transistor. The resistors in the $R_{TH\ ISO}$, $R_{TH\ AL}$, $R_{TH\ TIM}$ and $R_{TH\ CP}$ layers use an S_2 area which corresponds to the PCB surface. The resistor R_{Cu2} uses an area which is the difference between the areas S_2 and S_1 .

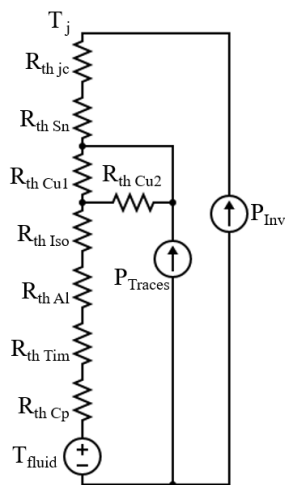


Fig. 14 Equivalent thermal circuit of the power PCB and heatsink.

The thermal resistance $R_{TH\ CP}$ was obtained by performing a CFD calculation of the heat sink. The exchange coefficient obtained is $1720\ W.m^{-2}.K^{-1}$ for a pressure of 260 Pa. With these parameters, the junction temperature of the transistors does not exceed $70\ ^\circ C$ in steady state for a fluid temperature of $40\ ^\circ C$. Even by multiplying the switching frequency by three, the junction temperature does not exceed $90\ ^\circ C$. The dimensioned heatsink therefore allows all the losses of the inverter to be evacuated while maintaining an acceptable temperature for the operation of the components.

5.6 IMMD final design

The IMMD designed using integration method C is shown in Figure 15. The converters are connected to the motor via a backplane to which the stator coils are soldered. Customised plug-in connectors have been developed to connect the modules to the backplane. The DC bus of the IMMD is made of a laminated busbar, on which additional capacitors for the DC-link are soldered. A resolver board is integrated on the stator backplane to

measure the rotor position for motor control. The total length of the IMMD is 160mm including connectors. The total volume of the IMMD is therefore $4534\ cm^3$, which represents a power density of $19.8\ W/cm^3$ for the motor power.



Fig. 15 3D CAD of the designed IMMD for the OW-PMSM.

6 Conclusion

An optimization method to design an IMMD for OW-PMSM has been presented. The electrical design of the inverter and the surface area required to implement it led to the selection of method C as the most suitable method for integration. Losses calculation for the selected transistors was performed using a calculation method based on the transistor parameters from their datasheet. Additional losses in the tracks of the power board were calculated from the CAD model of the power board. A total of 103 W of losses for the maximum operating point was calculated. According to the thermal model used, the losses represent a maximum temperature difference of $30\ ^\circ C$ for a switching frequency of 10 kHz. These electrical and thermal designs allow the IMMD to fit within the stator diameter for a maximum length of 160 mm. This represents a power density associated with the motor of $19.8\ W/cm^3$.

7 Reference

- [1] S. Runde, A. Baumgardt, O. Moros, B. Rubey and D. Gerling, "ISCAD — Design, control and car integration of a 48 volt high performance drive," in CES Transactions on Electrical Machines and Systems, vol. 3, no. 2, pp. 117-123, June 2019, doi: 10.30941/CESTEMS.2019.00017.
- [2] L. Dassonville, J. -Y. Gauthier, X. Lin-Shi, A. Makki, and A. Siccardi, "Availability analysis and quantification of electrical multiphase

- machines," IECON 2021 – 47th Annual Conference of the IEEE Industrial Electronics Society, Toronto, ON, Canada, 2021, pp. 1-6, doi: 10.1109/IECON48115.2021.9589456.
- [3] N. R. Brown, T. M. Jahns and R. D. Lorenz, "Power Converter Design for an Integrated Modular Motor Drive," 2007 IEEE Industry Applications Annual Meeting, New Orleans, LA, USA, 2007, pp. 1322-1328, doi: 10.1109/07IAS.2007.205.
- [4] A. Shea and T. M. Jahns, "Hardware integration for an integrated modular motor drive including distributed control," 2014 IEEE Energy Conversion Congress and Exposition (ECCE), Pittsburgh, PA, USA, 2014, pp. 4881-4887, doi: 10.1109/ECCE.2014.6954070.
- [5] J. Wang, Y. Li and Y. Han, "Integrated Modular Motor Drive Design With GaN Power FETs," in IEEE Transactions on Industry Applications, vol. 51, no. 4, pp. 3198-3207, July-Aug. 2015, doi: 10.1109/TIA.2015.2413380.
- [6] L. Verkroost, J. Van Damme, D. V. Bozalakov, F. De Belie, P. Sergeant and H. Vansompel, "Simultaneous DC-Link and Stator Current Ripple Reduction With Interleaved Carriers in Multiphase Controlled Integrated Modular Motor Drives," in IEEE Transactions on Industrial Electronics, vol. 68, no. 7, pp. 5616-5625, July 2021, doi: 10.1109/TIE.2020.2992965.
- [7] J. Van Damme, L. Verkroost, H. Vansompel, F. De Belie and P. Sergeant, "A holistic DC link architecture design method for multiphase integrated modular motor drives," 2019 IEEE International Electric Machines & Drives Conference (IEMDC), San Diego, CA, USA, 2019, pp. 1593-1598, doi: 10.1109/IEMDC.2019.8785391.
- [8] M. Schiestl, F. Marcolini, M. Incurvati, F. G. Capponi, R. Starz, F. Caricchi, A. S. Rodriguez et L. Wild, «Development of a High-Power Density Drive System for Unmanned Aerial Vehicles» IEEE Transactions on Power Electronics, vol. 36, p. 3159–3171, 3 2021.
- [9] M. Schiestl et al., "Development of a High Power Density Drive System for Unmanned Aerial Vehicles," in IEEE Transactions on Power Electronics, vol. 36, no. 3, pp. 3159-3171, March 2021, doi: 10.1109/TPEL.2020.3013899.
- [10] T. M. Jahns and H. Dai, "The past, present, and future of power electronics integration technology in motor drives," in CPSS Transactions on Power Electronics and Applications, vol. 2, no. 3, pp. 197-216, Sept. 2017, doi: 10.24295/CPSSTPEA.2017.00019.
- [11] G. -J. Su and L. Tang, "A segmented traction drive system with a small dc bus capacitor," 2012 IEEE Energy Conversion Congress and Exposition (ECCE), Raleigh, NC, USA, 2012, pp. 2847-2853, doi: 10.1109/ECCE.2012.6342375.
- [12] B. Rubey, A. Patzak, F. Bachheibl and D. Gerling, "DC-Link Current Harmonics Minimization in ISCAD Multi-Phase Inverters with Interleaving," 2017 IEEE Vehicle Power and Propulsion Conference (VPPC), Belfort, France, 2017, pp. 1-7, doi: 10.1109/VPPC.2017.8330880.
- [13] GRAOVAC, Dusan, PURSCHEL, Marco, et KIEP, Andreas. MOSFET power losses calculation using the data-sheet parameters. Infineon application note, 2006, vol. 1, p. 1-23.
- [14] M. Vujacic, M. Srndovic, M. Hammami and G. Grandi, "Evaluation of DC voltage ripple in single-phase H-bridge PWM inverters," IECON 2016 - 42nd Annual Conference of the IEEE Industrial Electronics Society, Florence, Italy, 2016, pp. 3235-3240, doi: 10.1109/IECON.2016.7793409.
- [15] NIE, Zipan et SCHOFIELD, Nigel. Multiphase VSI DC-link capacitor considerations. IET Electric Power Applications, 2019, vol. 13, no 11, p. 1804-1811.